Fusion Engineering and Design 213 (2025) 114872

Contents lists available at ScienceDirect

Fusion Engineering and Design

journal homepage: www.elsevier.com/locate/fusengdes

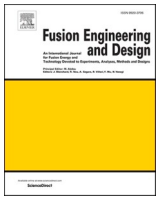

Dedicated thermo-mechanical analyses in support of DEMO HCPB BB design

Brahim Chelihi [a,*], Christophe Garnier [a], Julien Aubert [b], Guangming Zhou [c]

[a] CEA, DES, IRESNE, DTN, STCP, LCIT Cadarache, Saint-Paul-lez-Durance France
[b] CEA, DES, ISAS, DM2S, Saclay France
[c] Karlsruhe Institute of Technology (KIT), 76344 Eggenstein Leopoldshafen, Germany

ARTICLE INFO

Keywords:
DEMO
Breeding Blanket
HCPB
Thermo-mechanical
RCC-MRx

ABSTRACT

Within the framework of the EUROfusion Work Package Breeding Blanket for the fusion reactor DEMO, several concepts of Breeding Blanket (BB) are considered. One of the concepts being investigated is the Helium Cooled Pebble Bed (HCPB) BB.

The present study focuses on the assessment of this component from the steady-state thermal and thermo-mechanical point of view for Normal Operation conditions, with Finite Element Method Analysis and according to RCC-MRx criteria.

First design assessment revealed that the criteria were exceeded in three main areas. Design improvements in terms of mechanical performance are thus proposed and assessed.

The first area is the Side Wall and radius fillet. The reduction of the flow cross section, combined with the inward shifting of the First Wall cooling channels, allows compliance with the allowable stress (the maximal Eurofer temperature increase but remains below the limit of 550 °C). With regards to the allowable stress under irradiation, the suggested modifications do not enable the admissible value to be achieved and the wall thickness should be increased in the Side Wall area.

With regards to the second area, the manifold walls, the initial thickness of 10 mm enables the allowable stress to be satisfied, and this thickness should not be reduced. Increasing the manifold wall thickness does not allow to comply with the allowable stress under irradiation. A possible solution could be to rearrange the manifolds in order to achieve a more homogeneous temperature field and a reduction in thermomechanical stresses.

Concerning the pressure tube, increasing its thickness allows significant improvements and it would appear that a thickness of 10 mm is required to achieve the allowable stress under irradiation. However, increasing the pressure tube thickness will reduce the volume of the neutron multiplier and this could impact the Tritium Breeding Ratio.

1. Introduction

Within the framework of the European studies on the DEMO Breeding Blanket (BB) [1,2], several concepts are considered for possible implementation and are currently under development through different design phases [3]. One of the concepts being investigated is the Helium Cooled Pebble Bed (HCPB) BB.

Key component in Deuterium-Tritium fusion reactor, the BB allows the tritium breeding; multiplies the neutron; contributes to the nuclear shielding and extracts high-grade heat. The HCPB BB uses helium (80 bar) as coolant, lithium ceramic as tritium breeder (Advanced Ceramic Breeder - ACB), beryllium-containing material as neutron multiplier material (TiBe12), Eurofer97 as structural material and tungsten as armour (against plasma interaction and induced hot spots hazards) on the first wall (FW) [4].

The development of the BB goes through several phases, the present one being the Concept Design (CD, starting from 2021 to 2027). On basis of the studies performed during the previous phase (namely Pre-Concept Design, PCD) and their conclusions [5], significant improvements are proposed for the next phase in order to address the different identified issues:

* Corresponding author at. CEA, IRESNE, F-13108 Saint-Paul-lez-Durance, France.
E-mail address: brahim.chelihi@cea.fr (B. Chelihi).

https://doi.org/10.1016/j.fusengdes.2025.114872
Received 26 November 2024; Received in revised form 23 January 2025; Accepted 10 February 2025
Available online 16 February 2025

- Equalizing the purge gas pressure with the coolant pressure (80 bar) to resolve the low reliability issue,
- *Re*-arranging the manifold region to cool key structural components of the BB with cold helium,
- The connection rods at the Back Support Structure (BSS) regions are replaced with plates,
- Redesigning of the beryllide blocks from hexagonal to triangular prism (solid block shape improves structural integrity and reduce fabrication time) (described in Figure 2).

The EUROfusion HCPB BB team has iterated the design and produced a new version of the HCPB design from 2021 to 2023. Figures Fig. 1 and 2 compare the actual CD phase with the previous PCD one.

This new version has significantly evolved so that the global behaviour of the blanket should be assessed with especially neutronic, thermal, thermal-hydraulic and thermomechanical studies.

This article focuses on the thermal and thermo-mechanical analyses of an inboard HCPB BB equatorial slice (Fig. 3), according to the RCC-MRx structural design code rules [6] in order to justify its mechanical strength. Normal Operating (NO) conditions have been considered with criteria corresponding to Level A conditions and type P damages (monotonic loadings). In order to assess these criteria, a theoretical-numerical approach based on the Finite Element Method (FEM) has been followed. The commercial FEM code ANSYS [7] has been adopted.

Results are herewith presented for the new HCPB version and discussed. On basis of these conclusions, evolutions are then proposed and assessed. Finally, the follow-up of the design is detailed.

2. Methods

2.1. Criteria

Regarding the thermal and thermomechanical behaviors, two main points should be analyzed.

First, to guarantee the adequate mechanical properties, the Eurofer should not exceed 550 °C during the normal operation [8]. However, this temperature may be exceeded locally, in areas where the stresses are lower than the criteria.

Secondly, the mechanical design is evaluated according to the RCC-MRx structural design rules with the elastic analysis procedure. Here, normal operating conditions (NO) are considered thus leading to apply RCC-MRx Level A criteria. P-type failure, resulting from applying a constantly increasing load, has been considered. Associated rules cover the following damages: Immediate Excessive Deformation (IED) and Immediate Plastic Instability (IPI), taking into account the effect of irradiation on material structure. Resulting stresses are linearized and classified as primary, secondary and peak stresses. The first category with membrane and bending stresses, P_m and P_b respectively, is defined as the fraction of the total stress which does not disappear after small permanent deformation, commonly caused by imposed loads. Secondary stresses, with membrane and bending stresses, Q_m and Q_b respectively, is defined as the fraction of the total stress which can disappear as a result of small permanent deformation, minus the peak stresses, and are usually caused by thermal stresses, swelling stresses and stresses due to imposed displacements or deformations. Finally, peak stresses F is the fraction of the total stress which meets the following two conditions:

- It is the additional stress applied by a geometrical discontinuity of the structure or by non-linearity in the distribution of stresses within the thickness,
- This additional stress, generally very localized, cannot, should it be redistributed, cause deformation of the whole structure.

The sum of all these contributions gives the total stress.

Previous stresses or combined resulting stresses are compared to different criteria or allowable stresses, defined by the code for the different operating conditions and function of temperature (T) and for some cases irradiation (G). The applied criteria are detailed in Table 1 for level A criteria, where k_{eff} is equal to 1.5 for shells and plates, which is considered to be applicable for HCPB geometry. Case Negligible Irradiation (NI) does not take into account the effect of irradiation

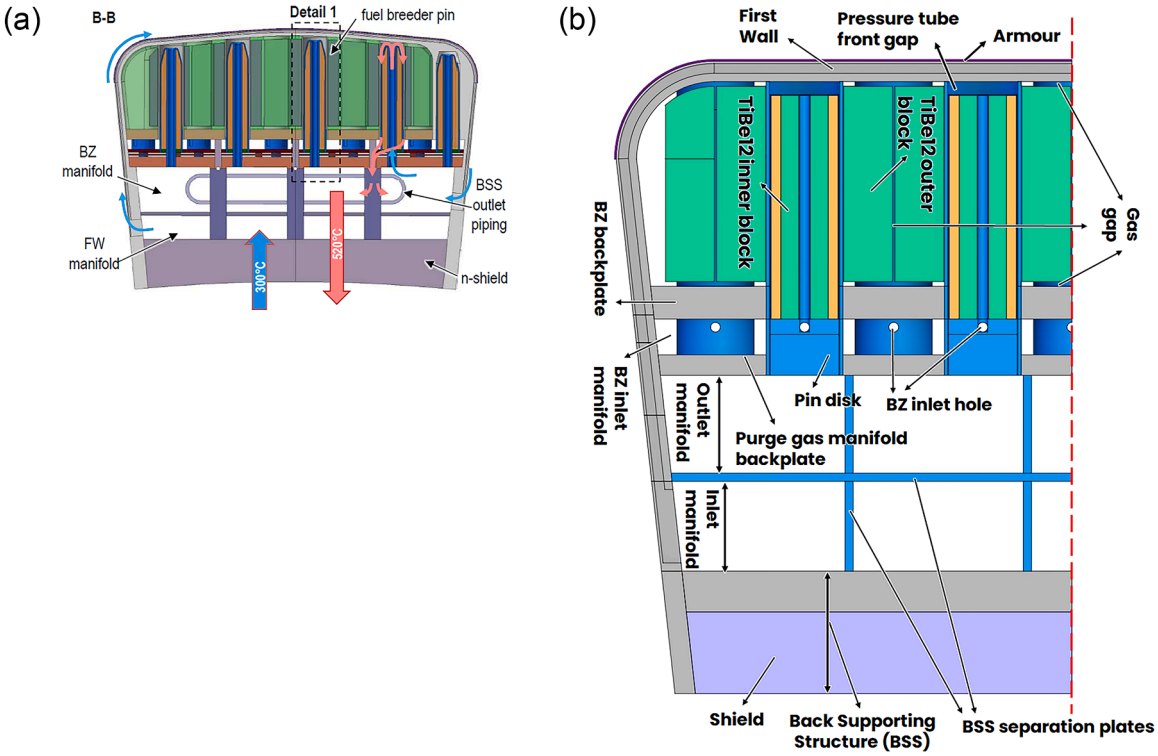

Fig. 1. View of HCPB BB inboard equatorial slice with its main components – a) PCD phase; b) CD phase.

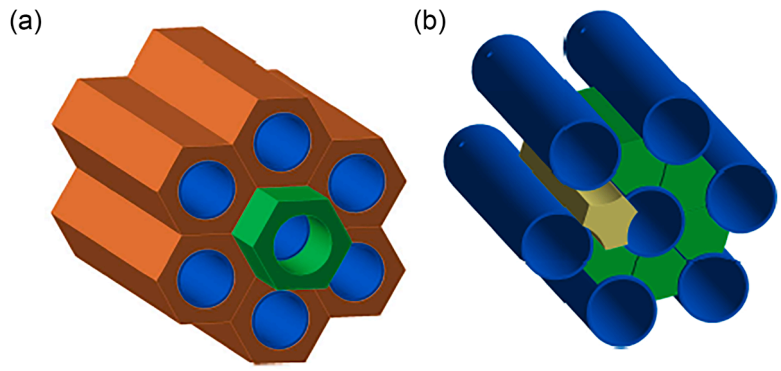

Fig. 2. View of TiBe blocks – a) Hexagonal prism (PCD phase); b) Triangular prism (CD phase).

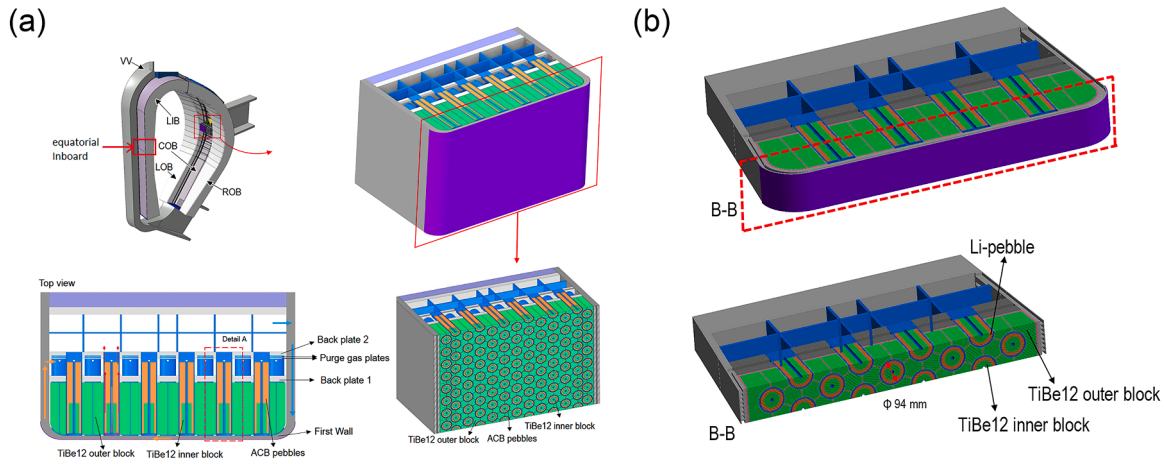

Fig. 3. Design of HCPB BB; a) Global view (Acronyms description: VV for Vacuum Vessel; LIB for Left InBoard; LOB for Left OutBoard; COB for Central OutBoard; ROB for Right OutBoard); b) Inboard blanket slice.

Table 1
RCC-MRx level A applied safety criteria for Type P damages.

	Criteria
Immediate Excessive Deformation (IED) without effect of irradiation (NI)	$\overline{P_m}/S_m^A(T) \leq 1$
Immediate Plastic Instability (IPI) without effect of irradiation (NI)	$\overline{P_m + P_b}/\left(k_{eff} \cdot S_m^A(T)\right) \leq 1$
Immediate Excessive Deformation (IED) with effect of irradiation (SI)	$\overline{P_m + Q_m}/S_{em}^A(T,\ G) \leq 1$
Immediate Plastic Instability (IPI) with effect of irradiation (SI)	$\overline{P_m + P_b + Q_m + Q_b + F}/S_{et}^A(T, G) \leq 1$

contrary to case Significant Irradiation (SI). Effects of time-dependent damages due to creep are not taken into account.

2.2. Analysis procedure

In order to validate the criteria presented in section 2.1, the analysis is carried out in two steps: a first thermal analysis is performed to calculate the heat transfer and the resulting temperature field in the structures; this first step is followed by a thermomechanical analysis taking into account the primary loads (essentially gas pressure) combined with the previously calculated temperature field.

Depending on the type of damage being investigated, the total (i.e. not linearized) equivalent stress is first basically compared to the corresponding relevant criteria. Whenever a criterion is not fulfilled, the stress is analysed in more detail using the linearization procedure. Areas where the equivalent stress exceeds the relevant criteria need to be analysed in more detail using linearized stresses. Design optimisations are required in areas where these linearized stresses do not satisfy all criteria.

These iterations on design are then successively performed until all criteria are reached.

2.3. Models

A numerical Finite Element (FE) model is set up to compute successively the thermal field (thermal model) and then the thermomechanical stress (thermomechanical model). The Finite Element (FE) Model corresponds to an Inboard equatorial unit slice (height 126 mm) of the HCPB BB (Fig. 3). A symmetry condition is applied along the radial-poloidal plane (as shown in Fig. 4) so that only half geometry is modelled. It should be noted that this assumption is not correct for the FW cooling channels, as the fluid temperature evolution is not symmetric. However, this simplification is not expected to affect the results. Finally, the behaviour is simplified and considered to be linearly periodic along the poloidal axis (infinite linear repetition of the slice along the poloidal axis, segment curvature is not taken into account).

2.3.1. Thermal model

The thermal FE model includes all components that influence the heat transfer: Eurofer structure, ACB, TiBe blocks and the tungsten armour (2 mm thickness) as presented in Fig. 4. Heat transfer between fluid (He gas) and structure is also taken into account. For this thermal model, 3,513,812 linear elements with 2,257,361 nodes are used.

The two thermal loads considered are:

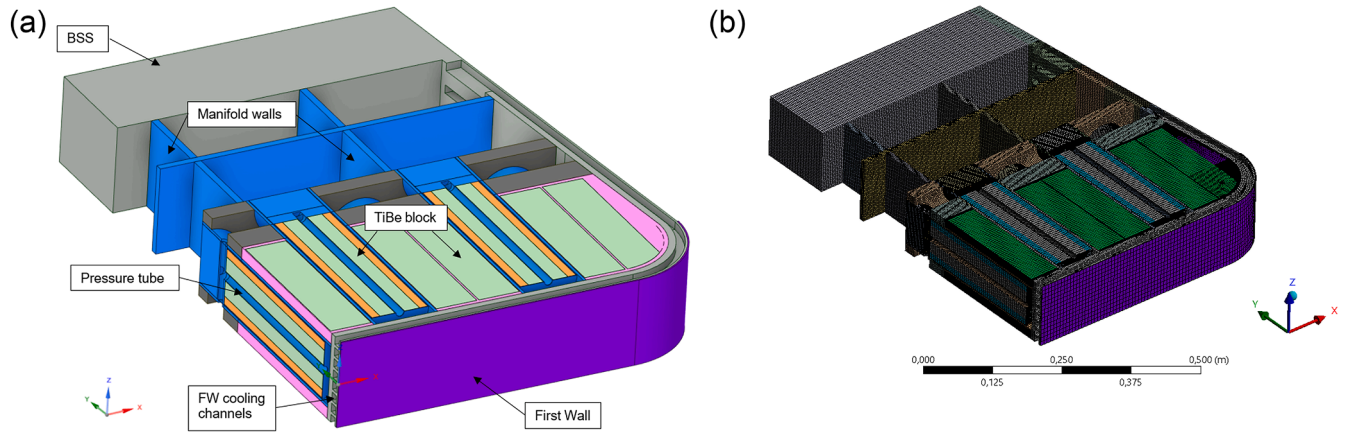

Fig. 4. Thermal FE model; a) Global view; b) Thermal FE mesh.

- The plasma heat flux on FW face (applied as a constant value of 0.25 MW/m^2),
- The nuclear heating (as volumetric heating), depending on both, the material and the radial position.

All other faces are adiabatic.

The HCPB BB is cooled by helium at 80 bar. The coolant enters in the FW at 300 °C from the inlet manifold, with a manner of alternating flow direction in the adjacent channels to achieve a more uniform temperature and symmetric distribution. After cooling down the FW, the coolant is collected via the Breeding Zone (BZ) inlet manifold. Subsequently, the coolant is distributed into the fuel-breeder pins. Following the cooling of the fuel-breeder pins, the coolant is collected in the BSS outlet manifold. The corresponding flow rate is determined to achieve the following coolant temperatures: 300 °C, 385 °C and 520 °C for the FW inlet, the BZ inlet and the BB outlet temperature respectively.

The model uses fluid-type elements (Fluid116 elements) to simulate the heat exchange between the fluid and the structure along the flow path. These elements are employed for all cooling channels without the resolution of Navier-Stokes equations incorporating the effects of heat exchange (heat exchange coefficient between fluid and wall is imposed).

2.3.2. *Thermomechanical model*

The thermomechanical FE model is presented in Fig. 5. Only the Eurofer structure is taken into account (FW, Side Wall (SW), pressure tubes, BSS manifold) since it insures the mechanical integrity and tightness of the BB. The tungsten layer is not represented in the model, so there is no induced thermal stress with the FW. For this thermomechanical model, 1,689,244 quadratic elements with 4,628,808 nodes are used.

The corresponding applied loads are:

- A gas (He) pressure of 80 bar was applied to all coolant and purge gas wetted surfaces, as depicted in Fig. 6,
- The temperature field was imported from the previous thermal calculation.

The thermomechanical boundary conditions are detailed in Fig. 7.

A symmetry condition is applied to the face representing the middle of the slice (X axis). A flatness condition is applied to the upper surface, whereas the lower surface is constrained along the poloidal axis (Z axis). Finally, the rear surface of the BSS is constrained along the radial direction (Y axis).

These boundary conditions globally overestimates the model stiffness. However, this practice is commonly used for similar studies, where the conservativeness of the approach allows a good compromise between calculation cost and accuracy of the results.

Once the stress field is calculated for all the assumed loading scenarios, a stress linearization procedure has been performed along paths located within the most stressed regions of the IB segment.

3. Initial design assessment & modifications

3.1. *Initial design*

As previously explained, EUROfusion HCPB BB team has designed a new evolution of the PCD phase, which serves as the initial design for the different performance assessments, which include present

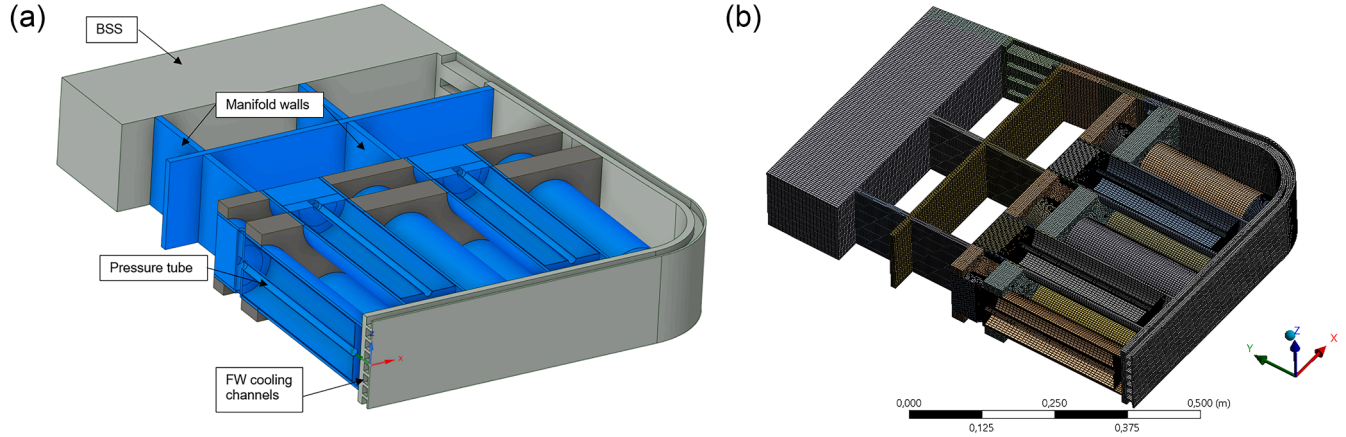

Fig. 5. Thermomechanical FE model; a) Global view; b) Thermomechanical FE mesh.

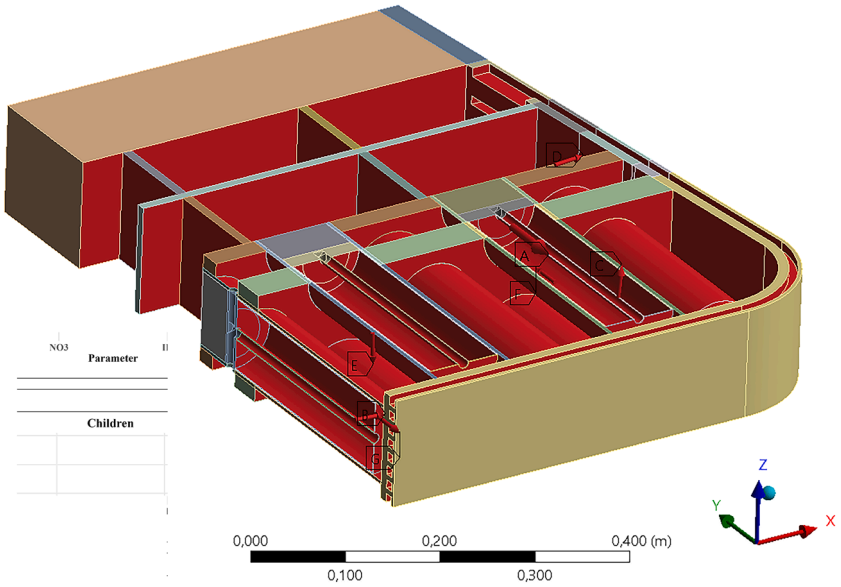

Fig. 6. Surfaces submitted to gas pressure (80 bar).

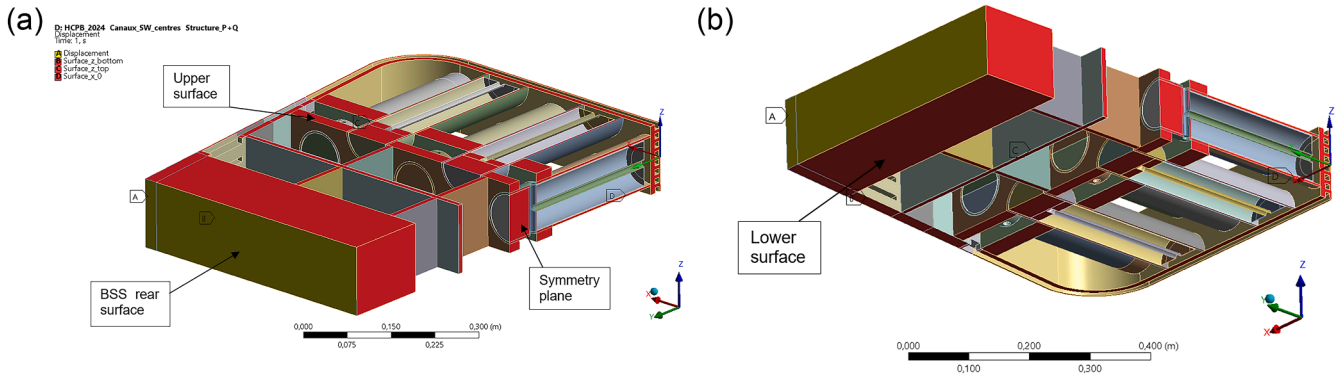

Fig. 7. Thermomechanical boundary conditions; a) Top view; b) Bottom view.

thermomechanical analysis. The main modifications with regards to the PCD phase have been described in Section 1. The delivered geometry (next named as "initial design") is depicted in Fig. 8.

There are 8 FW cooling channels (6 with full cross section and 2 half channels) across the slice. For the initial design, the FW cooling channels cross section is 12×12 mm^2. The external thickness (distance between channels and the tungsten armour) is 3 mm whereas the internal thickness is 10 mm and the distance between two adjacent walls is 4.5 mm.

A 3 mm gap is incorporated between the TiBe12 blocks to limit the temperature increase and facilitate purge gas flow. To prevent a significant heat transfer from the TiBe12 blocks to the pressure tube, a 1 mm gap has been incorporated into the design.

3.2. First thermal results

A first thermal evaluation of this version has been performed with a maximum EUROFER temperature of 573 °C (see Fig. 9). This evaluation also serves as thermal loading for the following thermomechanical analysis. Despite the exceeding of the maximum Eurofer temperature (550 °C, see 2.1), this design has been considered as acceptable from the thermal point of view. Indeed, this maximum value is close to the value of 550 °C and is very localised. Moreover, the thermomechanical stresses in this area are negligible.

3.3. First thermomechanical results

For this purpose, the previously described thermomechanical model has been applied to compute the elastic stresses used to assess the RCC-MRx criteria.

In order to illustrate the effect of NO pressure, Fig. 10 presents both the displacements and deformed shape under pressure loading. It highlights the SW and manifold walls bending, suggesting that these areas may require detailed analysis.

First preliminary analysis is based on the comparison of the equivalent Von Mises stress (not linearized) to the applicable criteria. As described in section 2.2, areas where the ratio on membrane stress exceeds unity (i.e. $S_{eqv} > S_m^A$ or $S_{eqv} > S_{em}^A$) requires detailed analysis, with stress linearization. Fig. 11 presents this ratio for both pressure loading (with S_m as allowable stress), and pressure loading associated with thermal loading (thermal stress, with S_{em} as allowable stress). It highlights several areas that exceed the criteria on membrane stress (SW and FW radius fillet, manifolds, lateral pressure tube) requiring further analysis on well-chosen paths. Selected paths as well as detailed analysis results are described in Fig. 12 and Fig. 13. Regarding FW and SW channels, paths have been located either through the whole wall thickness or through the channel walls, since they are subjected to internal pressure.

The ratio of linearized stress results in regards to stress limit are detailed in Fig. 14.

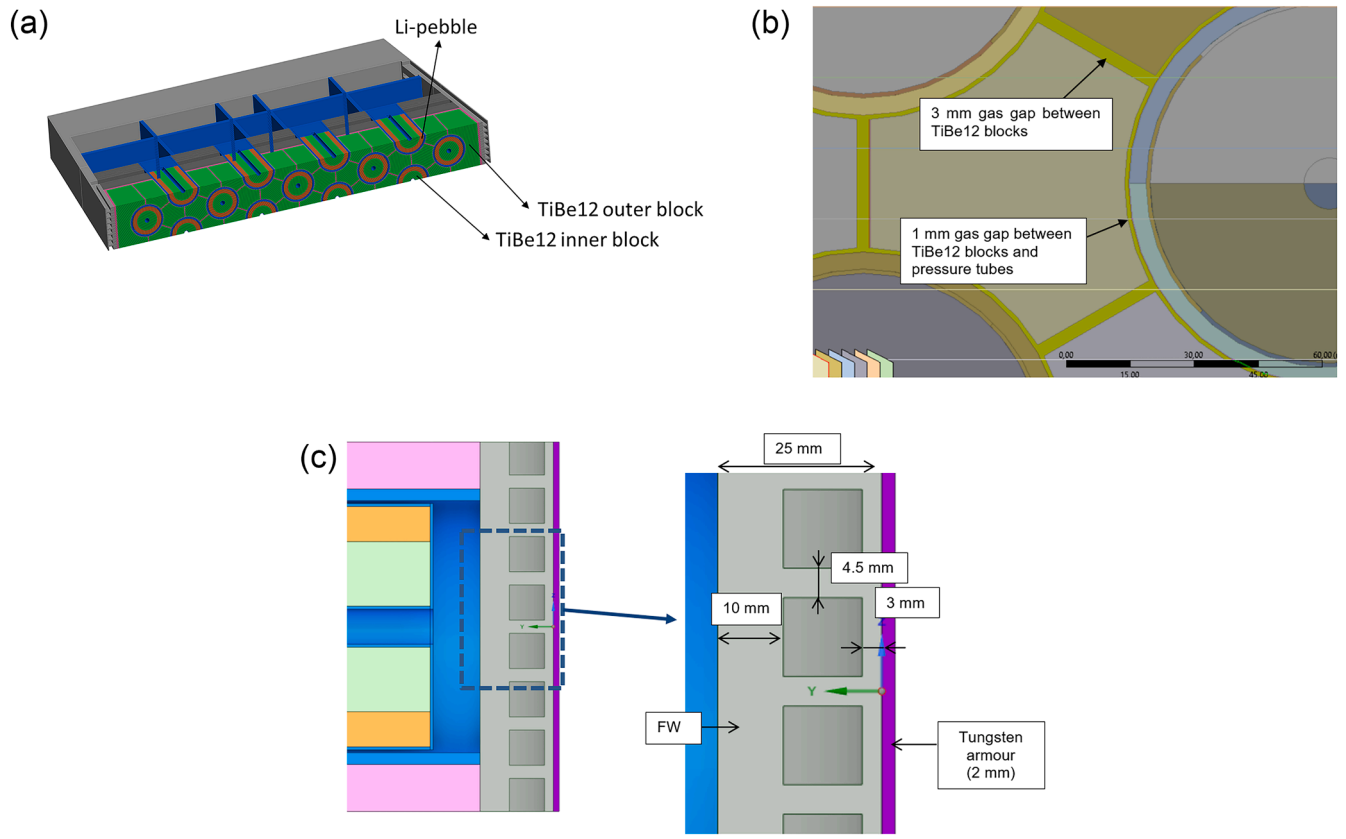

Fig. 8. Initial HCPB design (CD phase, slice); a) TiBe block view; b) Hexagonal prism view (gas gap details); c) FW cooling channels view.

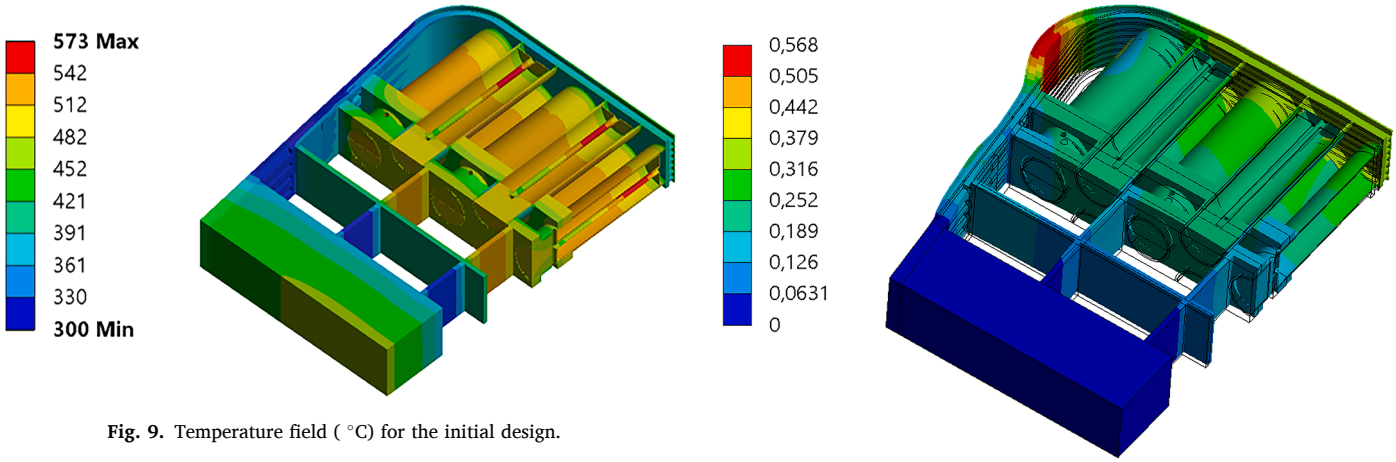

Fig. 9. Temperature field (°C) for the initial design.

Primary stress respects mainly the criteria on S_m except on the SW, where the bending is the highest.

When taking into account thermal stress, nearly all selected paths exceed the membrane criterion S_{em}. The other criterion on the total stress $\overline{P_m + P_b + Q_m + Q_b + F}$ is respected with significant margin and is not detailed.

On basis of the previous results, it can be concluded that the initial geometry requires modifications, which can be driven by the previous analyses. Primary stress which does not respect criteria on S_m suggests that the stiffness should be increased with for instance increasing the thickness or adding additional walls. On the other hand, secondary stress requires either to reduce thermal gradients (homogenizing the thermal field) or to improve the flexibility. Among these options, reducing the thermal gradients would mean modifying the cooling layout and is not favoured presently. Therefore, the main effort will be concentrated on geometry modifications.

Fig. 10. Deformed shape (x85) and elastic displacement (mm) for the initial design under pressure loading.

The bending of the SW and FW radius fillet is important despite the manifold wall, as it can be seen in Figure 10, and the primary stress $\overline{P_m + P_b}$ exceeds the criteria on S_m. This area also exceeds the criterion on primary and secondary stress S_{em}. The reducing of the SW bending may help to improve this later stress, but may be insufficient, so that the thermal field should be also modified. As a first step, only limited geometry modifications are favoured. The shift of the FW cooling channels through the wall thickness is one simple possibility that could reduce the thermal gradients. Another tested option is the reduction of their hydraulic section which will increase the total structural wall thickness (without any consideration on pressure loss impact).

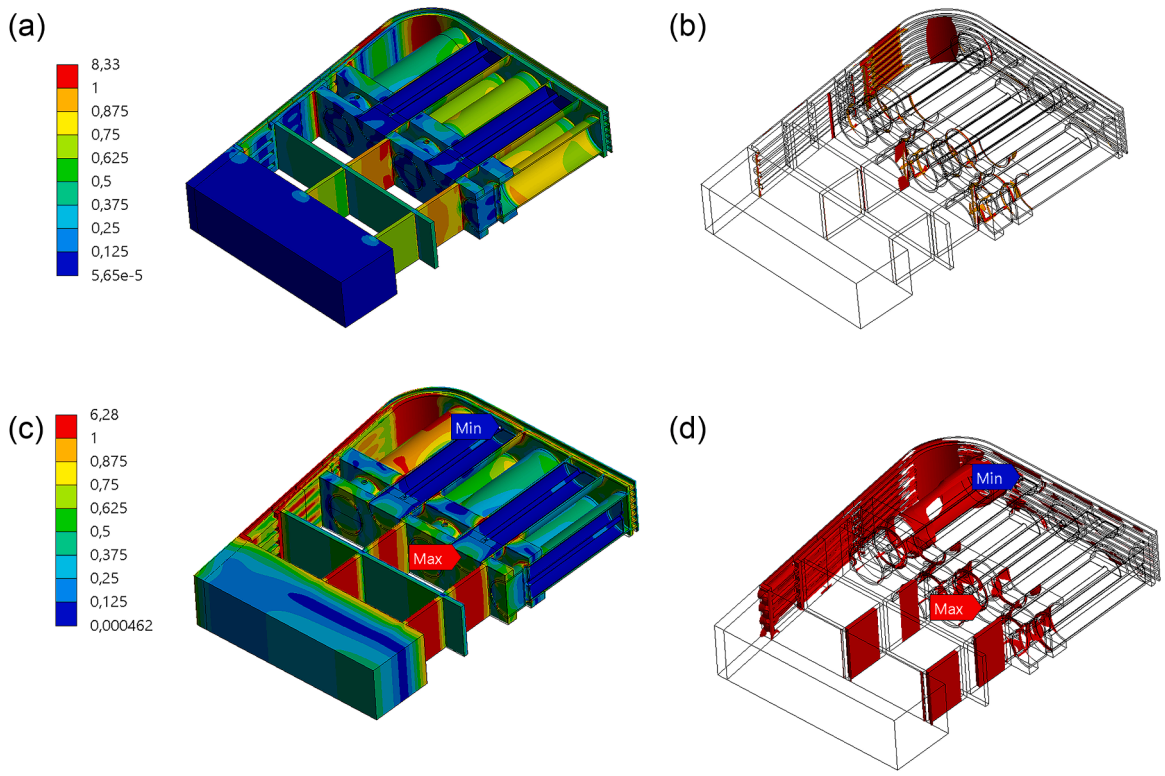

Fig. 11. a) Pressure loading - ratio $S_{eqv}/S_m(T)$; b) Pressure and thermal loading – ratio $S_{eqv}/S_{em}(T,G)$.

Regarding the manifold walls, the criterion on primary and secondary stress S_{em} is exceeded. The first and simplest option would be to modify the geometry in order to gain margin on primary stress with either increasing their thickness or adding new plates.

Finally, the lateral pressure tube wall does not respect the criterion on primary and secondary stress S_{em}. As for the manifold walls case, the first option is to modify the tube thickness, without any consideration on secondary stress.

The different previous proposed modifications are assessed in the next section.

4. Modifications assessment

According to the previous results, the following different parts of the blanket are successively studied: the SW, the manifolds and the pressure tube. Similar paths are used for linearization as for initial design.

4.1. SW cooling channels

As explained in the previous section 3.3, the criteria on S_m and S_{em} are exceeded on SW and FW radius fillet.

This paper will focus only on two modification assessments: first the cooling channel position across the wall thickness and secondly its cross section (as described in Table 2 and Fig. 15). These design optimisations apply to the FW, the SW and the radius fillet (hereafter referred to as FSW).

Please note that the external thickness corresponds to the distance between a cooling channel and the tungsten armour according to Figure 8. Furthermore, the flow cross section has been changed to maintain a square section.

The resulting temperature fields corresponding to these modifications are globally very similar to the one calculated for the initial design in Figure 9. However, as the modifications are located in the areas where the nuclear heating is the highest, some slight differences are observed and shown in Fig. 15. The design with the centred and reduced channels generates an increase of 64 °C compared with the initial design (464 °C for 528 °C), but this value is still below 550 °C.

For each of the proposed modifications, the temperature differences and the thermal gradients along the paths studied are detailed in tables Table 3 and Table 4 respectively (the results in red represent the cases where the result is worse than for the initial design). The temperature difference increases with wall thickness due to nuclear heating. The highest temperature difference increase is on the radius fillet outer area (from 30.0 °C to 76.7 °C for RF_2). Concerning the thermal gradients, they remain globally stable for the centred channels version: the increase of thickness probably balances the temperature difference rise. Some high increase are observed for the second version (centred version) on radius fillet: in this case, due to very high nuclear heating, the temperature rise is not balanced by the thickness increase. Finally, they globally increase for the last modified version.

The increase of temperature has an impact on the criteria value (decrease when the temperature increases), whereas thermal gradients have effect on thermal stress (increases when the thermal gradient increases).

The ratios of linearized primary stress on S_m are detailed in tables 5 and 6 for each cases under study.

As described in Figure 12, SW_4 and SW_6 correspond to the outer channel wall and to the distance between two adjacent walls respectively.

Concerning the primary membrane stress $\overline{P_m}$ on SW_4 (external wall thickness), the ratio decreases as the wall thickness increases (from 3.0 mm to 7.5 mm). Based on the curve presented in Fig. 16, it can be assumed that a minimum wall thickness of 7 mm may be necessary to achieve a ratio $\overline{P_m}/S_m$ below unity. Conversely, the ratio on SW_5 (internal wall thickness) increases with decreasing thickness, but the margin remains very high.

With regards to the area between two adjacent walls (SW_6), it is demonstrated that an increase in wall thickness from 4.5 mm to 6.5 mm (by reducing the cross section from 12×12 mm² to 10×10 mm²) allows to comply with the membrane criterion $\overline{P_m}$ on S_m.

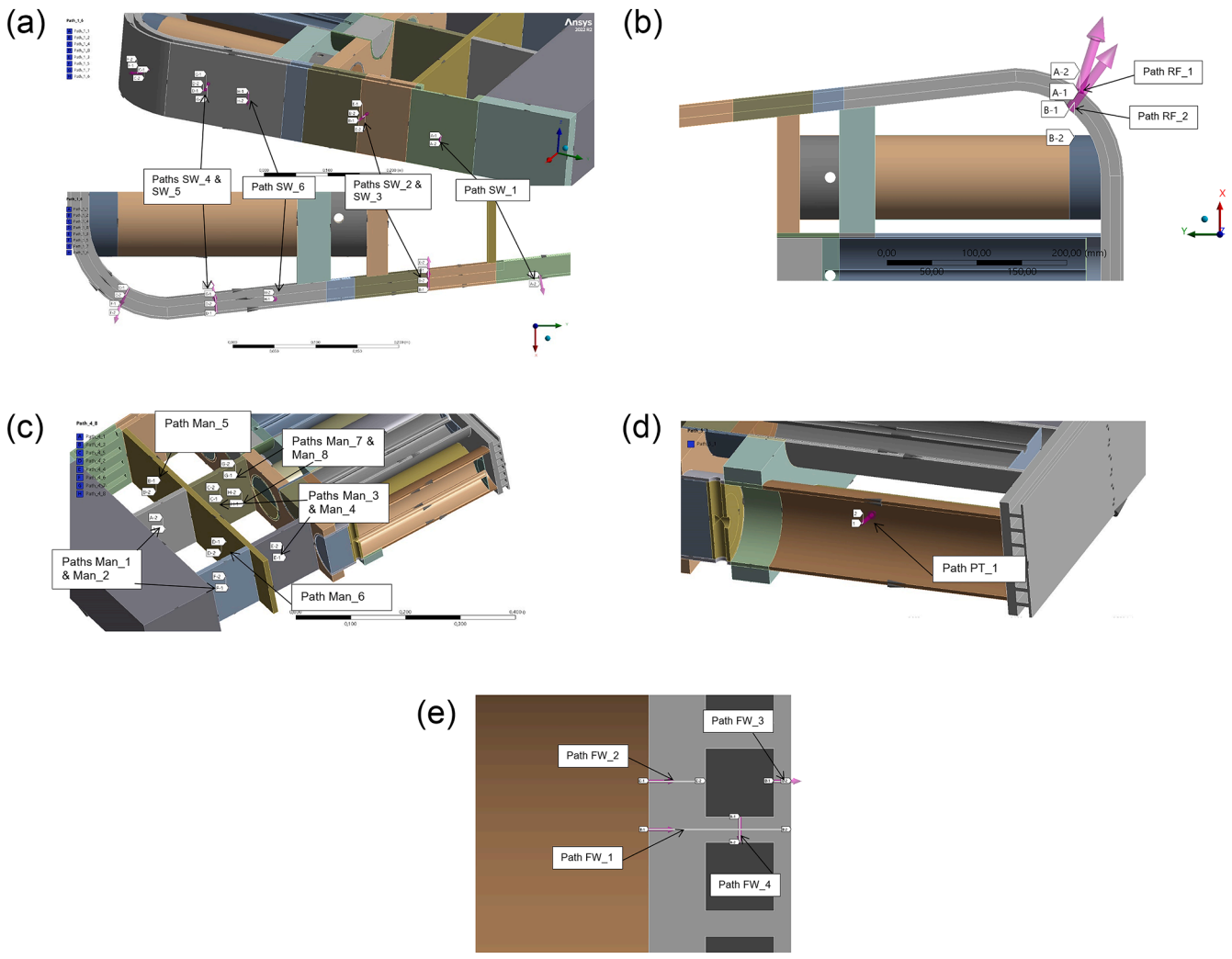

Fig. 12. Primary stress linearization paths – a) SW (SW_); b) FW Radius fillet (RF_); c) Manifolds (MAN_); d) Pressure tube (PT_); e) FW (FW_).

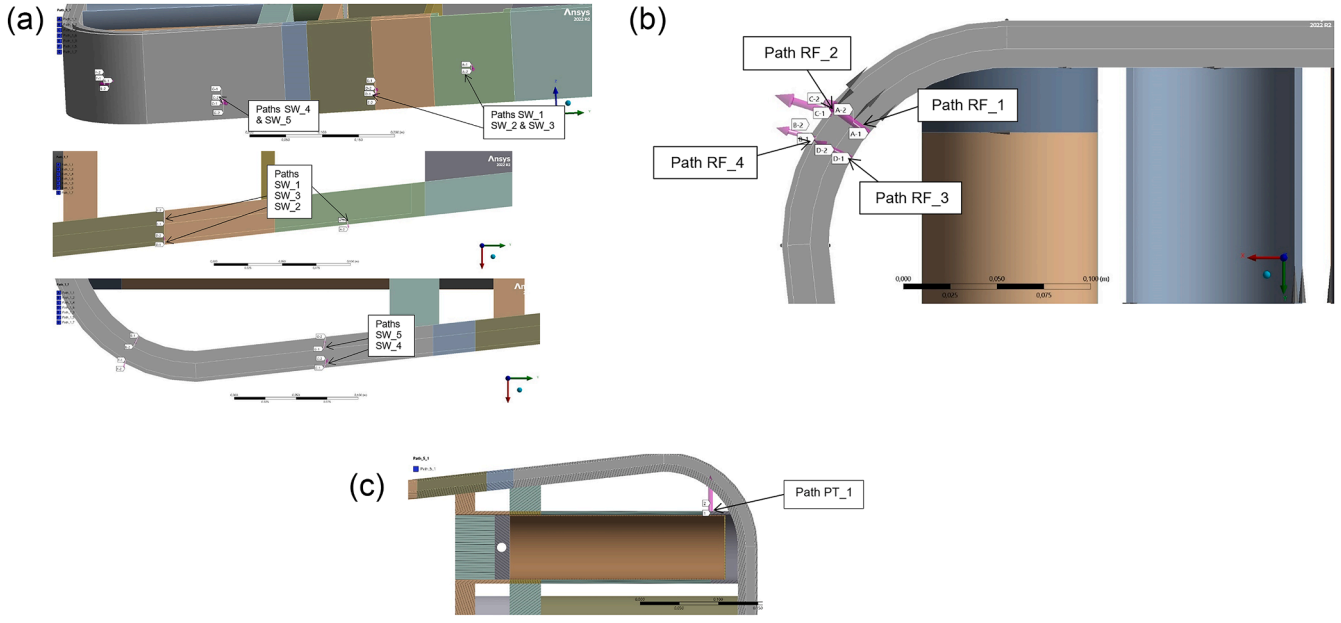

Fig. 13. Primary and secondary stress linearization paths – a) SW (SW_); b) FW Radius fillet (RF_); c) Manifolds (MAN_); d) Pressure tube (PT_).

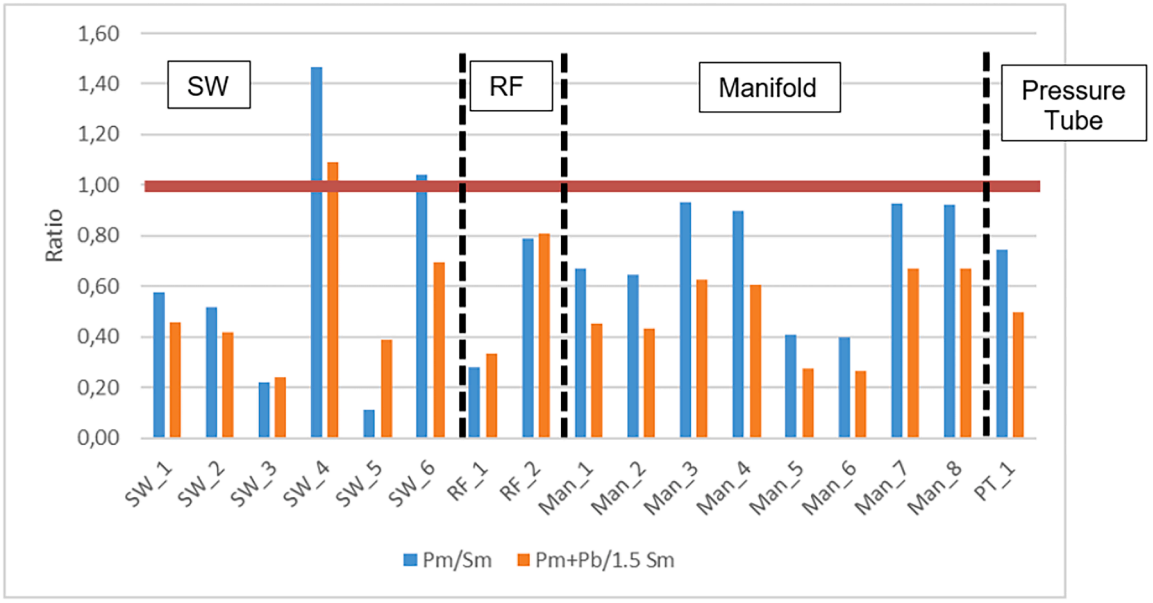

Fig. 14. Linearization results for initial HCPB version – a) Primary stress; b) Primary and secondary membrane stress.

Table 2
FSW cooling channels – design modifications.

	FSW Internal thickness [mm]	FSW External thickness [mm]	Flow cross section [mm²]	Distance between two adjacent walls [mm]
Initial design	10	3	12×12	4.5
Centred channels (slightly shifted inward)	6.5	6.5	12×12	4.5
Reduced channels	11	4	10×10	6.5
Reduced and centred channels	7.5	7.5	10×10	6.5

Furthermore, all the studied design optimisations enable compliance with the primary stress $\overline{P_m + P_b}$ criterion on S_m.

Finally, the case with reduced and centred FW cooling channels allows to comply with RCC-MRx rules when thermal loads are not taken into account (a slight increase of thickness may be needed for reduced channels configuration).

The ratio between primary and secondary membrane stress and S_{em} is detailed in Table 7 for each case under study. The red colour indicates that the RCC-MRx criterion is exceeded and the arrows point if the values increase with regards to the initial design.

It can be observed that there is a general improvement in the results

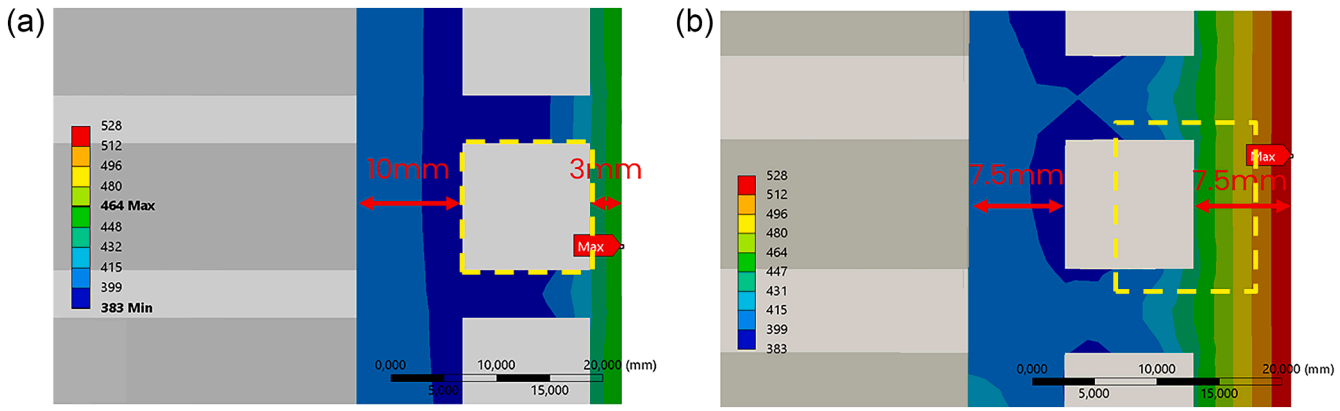

Fig. 15. Thermal field (°C) around FW channels; a) Initial design; b) Reduced and centred channels design.

Table 3
Temperature difference along studied paths (°C) – FSW channels.

path	Initial design	Centred channels	Reduced channels	Reduced and centred channels
SW_1	0.2	0.8	0.8	1.1
SW_2	1.4	3.1	3.1	5.1
SW_3	31.8	20.8	20.8	24.6
SW_4	4.5	11.8	11.9	14.9
SW_5	18.9	12.5	12.2	15.7
SW_6	20.7	21.1	21.1	28.2
RF_1	27.4	16.3	16.3	21.7
RF_2	30.0	64.2	64.2	76.7
RF_3	25.7	15.2	15.2	20.0
RF_4	27.2	57.8	57.8	67.7

Table 4
Thermal gradient along studied paths (°C/m) – FSW channels.

path	Initial design	Centred channels	Reduced channels	Reduced and centred channels
SW_1	0.06	0.12	0.19	0.15
SW_2	0.45	0.48	0.78	0.67
SW_3	3.18	3.20	1.89	3.28
SW_4	1.51	1.82	2.97	1.98
SW_5	1.89	1.92	1.11	2.09
SW_6	4.61	4.70	3.25	4.34
RF_1	2.74	2.51	1.48	2.89
RF_2	9.99	9.88	16.05	10.23
RF_3	2.57	2.34	1.38	2.67
RF_4	9.07	8.90	14.46	9.03

Table 5
$\overline{P_m}/S_m(T)$ – FSW channels.

path	Initial design	Centred channels	Reduced channels	Reduced and centred channels
SW_1	0.58	0.49	0.54	0.47
SW_2	0.52	0.45	0.48	0.13
SW_3	0.22	0.19	0.21	0.20
SW_4	1.47	1.06	1.20	0.94
SW_5	0.11	0.30	0.13	0.29
SW_6	1.04	1.08	0.76	0.80

when the FW cooling channels are shifted slightly inward (centred channels), with the exception of the radius fillet internal side (RF_1 and RF_3), due to the reduction in wall thickness. For RF_1 and RF_3 paths, the primary membrane stress is predominant and the secondary stress has a negligible impact as the thermal gradient remains stable (as shown in Table 4).

Concerning RF_2 and RF_4 and especially for the reduced centred version (for which the thermal gradient is highly increased suggesting that the ratio should increase), the ratio is reduced with same explanation as previous one (primary stress is probably predominant).

Table 6
$\overline{P_m + P_b}/1.5S_m(T)$ – FSW channels.

path	Initial design	Centred channels	Reduced channels	Reduced and centred channels
SW_1	0.46	0.36	0.39	0.37
SW_2	0.42	0.34	0.35	0.32
SW_3	0.24	0.20	0.24	0.20
SW_4	1.09	0.89	0.92	0.82
SW_5	0.39	0.37	0.39	0.38
SW_6	0.70	0.73	0.51	0.54

Reducing the flow cross section improves the results on all paths, but the criterion is still not satisfied. The influence of this modification on SW_1 and SW_2 is very low. The total wall thickness in this area could probably be increased: indeed, since the nuclear heating is lower here, the need to cool down the structure is reduced.

Finally, the combination of reducing the flow cross section and moving inward the channels induces also improvements on all linearized paths, except on SW_3 (slightly), RF_1 and RF_3.

Further investigations into reducing the flow cross section of the FW cooling channels may be beneficial, possibly combined with local increases in total FSW wall thickness near SW_1 and SW_2. However, it is important to note that a further reduction in the cooling channel section could result in a significant rise in the local maximal temperature of the FW (as well as an increase of pressure loss).

As previously mentioned, another option to investigate would be the introduction of a stiffening plate to decrease the SW wall bending stress as described in Fig. 17.

4.2. Manifold walls

As previously indicated in section 3.3, the criterion on S_{em} is exceeded on manifold walls. The objective of this section is to assess the impact of varying the thickness of the manifold walls on the primary and secondary membrane stress $\overline{P_m + Q_m}$. In addition, the number of manifold walls has been increased.

Given the direct impact of manifold wall thickness on primary membrane stress $\overline{P_m}$ and the low margin on the criterion S_m, this quantity has also been studied.

The thermal field presented in Figure 9 shows that the temperature across the wall remains constant for plates which exceed the criterion (for initial design but also for other designs). Therefore, secondary membrane stress do not result from this. The average temperature across inlet (MAN_1 and MAN_2) and outlet (MAN_3 and MAN_4) manifold

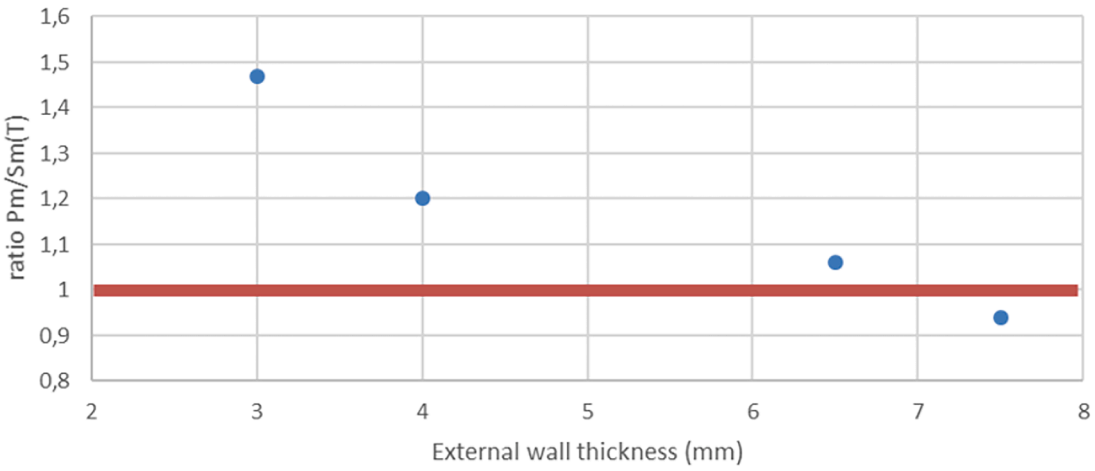

Fig. 16. Evolution on the ratio $P_m/S_m(T)$ depending on the FSW external wall thickness (SW_4).

Table 7
$\overline{P_m + Q_m}$/Sem(T,G) – FSW channels.

path	Initial design	Centred channels	Reduced channels	Reduced and centred channels
SW_1	1.86	1.63 ↘	1.80 ↘	1.58 ↘
SW_2	1.91	1.58 ↘	1.76 ↘	1.49 ↘
SW_3	1.02	1.16 ↗	0.97 ↘	1.09 ↗
SW_4	1.81	1.09 ↘	1.29 ↘	0.98 ↘
RF_1	1.25	1.77 ↗	1.13 ↘	1.64 ↗
RF_2	0.86	0.54 ↘	0.76 ↘	0.58 ↘
RF_3	1.33	1.84 ↗	1.20 ↘	1.72 ↗
RF_4	1.03	0.61 ↘	0.88 ↘	0.63 ↘

walls is 311 °C and 522 °C respectively, which correspond thus to the associated wall temperature.

The variation of the ratio $\overline{P_m}/S_m$ depending on the manifold wall thickness is presented in Fig. 18. Only the results corresponding to path MAN_3 are presented (conservative results).

The manifold wall thickness in the initial design is 10 mm and calculations have been performed for 7, 8 and 12 mm. As the thickness of the manifold wall increases, the margin also rises (primary stress decreases with thickness). However, for wall thickness from 8 mm and below, the criterion is no longer respected.

To assess the impact of the number of panels, an additional calculation was performed with eight panels (previously four) and a thickness of 10 mm (see Fig. 19). The result is also presented in Figure 18 indicated by the green mark. An increase in the number of plates while maintaining the same wall thickness results in a reduction of the ratio $\overline{P_m}/S_m$ (and therefore an increase in the margin) from 0.93 to 0.57 (same effect and reason as increasing the plate thickness).

The criterion on primary stress $\overline{P_m + P_b}$ has also been studied, but will not be included this paper (it is reminded that the associated criterion is satisfied with the initial design).

The ratio between primary and secondary stress and S_{em} is detailed in Table 8 for different values of manifold wall thickness. The red colour indicates that the criterion is exceeded.

As for the previous results, the ratio decreases with increasing thickness due to the reduction of the primary part in the sum. However, the variations are negligible and the results remain above the required values. This can be attributed to the prevalence of secondary stresses (of thermal origin) over primary stresses. Adding others stiffening plates has no impact on the results.

It can be concluded that the thickness of the manifold walls and the addition of plates do not represent an efficient solution in this case.

However, given the proximity between the hot and cold manifolds, rearranging them would result in a more homogeneous temperature field (along the radial axis) and a reduction in thermomechanical

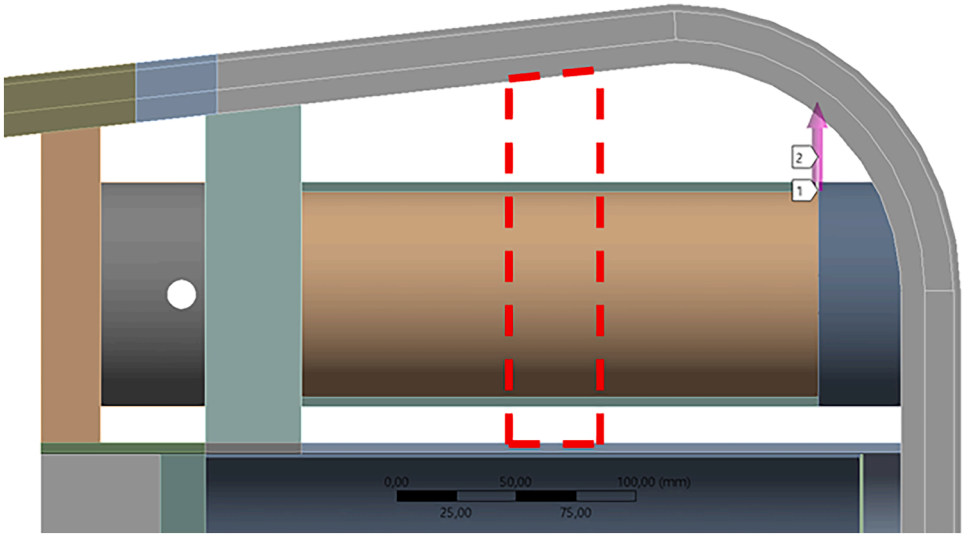

Fig. 17. Further study in progress – introduction of a new stiffening plate.

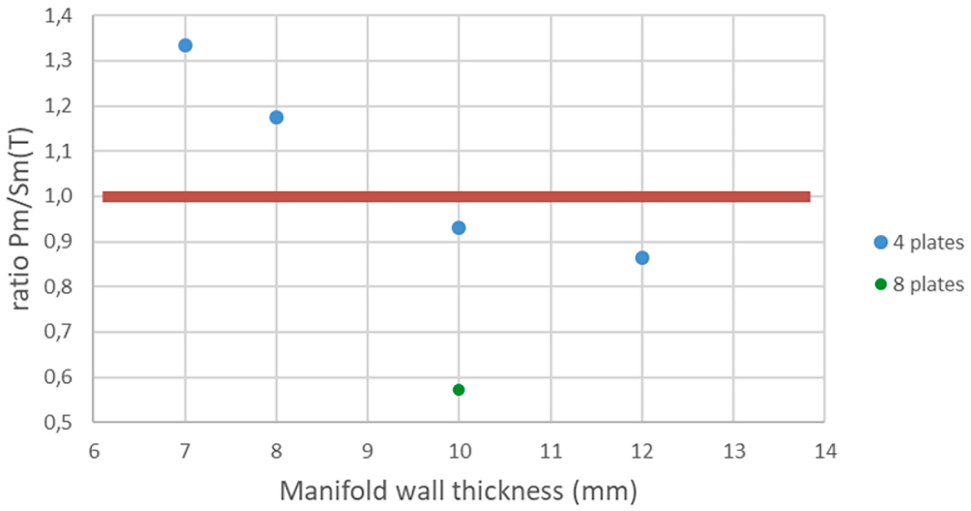

Fig. 18. Evolution of the ratio $P_m/S_m(T)$ depending on the manifold wall thickness (MAN_3).

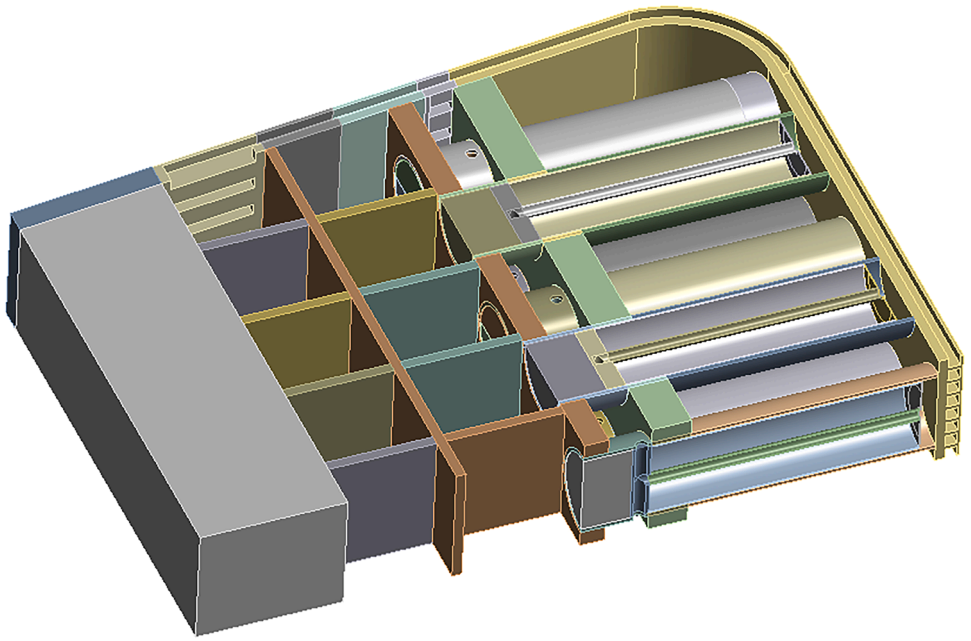

Fig. 19. 8 manifold plates (10 mm wall thickness).

Table 8
Primary and secondary stress $\overline{P_m + Q_m}$/Sem(T,G) – Manifold walls.

Path	th = 7 mm	th = 8 mm	th = 10 mm (initial design)	th = 12 mm	th = 10 mm +4 plates
MAN_1	1.37	1.31	1.27	1.23	1.25
MAN_2	1.41	1.34	1.28	1.24	1.25
MAN_3	1.09	1.08	1.04	1.04	1.05
MAN_4	1.24	1.22	1.13	1.12	1.11

stresses. To obtain a more homogeneous temperature field, the following rearrangement of the manifold (from the FW to the BSS) could be considered: the outlet manifold, the intermediate manifold and the inlet manifold.

As explained previously, the secondary membrane stress does not result from thermal gradient across the wall thickness, but rather from the temperature field which is not homogeneous, especially along the radial axis. The inlet manifold (MAN_1 and MAN_2) is colder than the outlet manifold (MAN_3 and MAN_4) and BSS. This configuration leads to increase thermomechanical stresses on inlet manifold walls: inlet manifold is submitted to traction thermal stress, while outlet manifold presents compressive stress. Similarly, the outlet manifold is hotter than the inlet and intermediate manifolds.

This phenomenon is highlighted in Fig. 20, which shows the vector principal stress. Red and blue vectors represent areas where the structure works in traction and compression respectively. As expected previously, the inlet and outlet manifold walls work in traction and compression respectively.

In addition, the flatness condition on the upper face averages the node displacements (along poloidal axis Z) due to the thermal expansions. This boundary condition restricts the thermal expansion of hot areas (front BB area, compression), while enhancing that of cold areas (back BB area, traction).

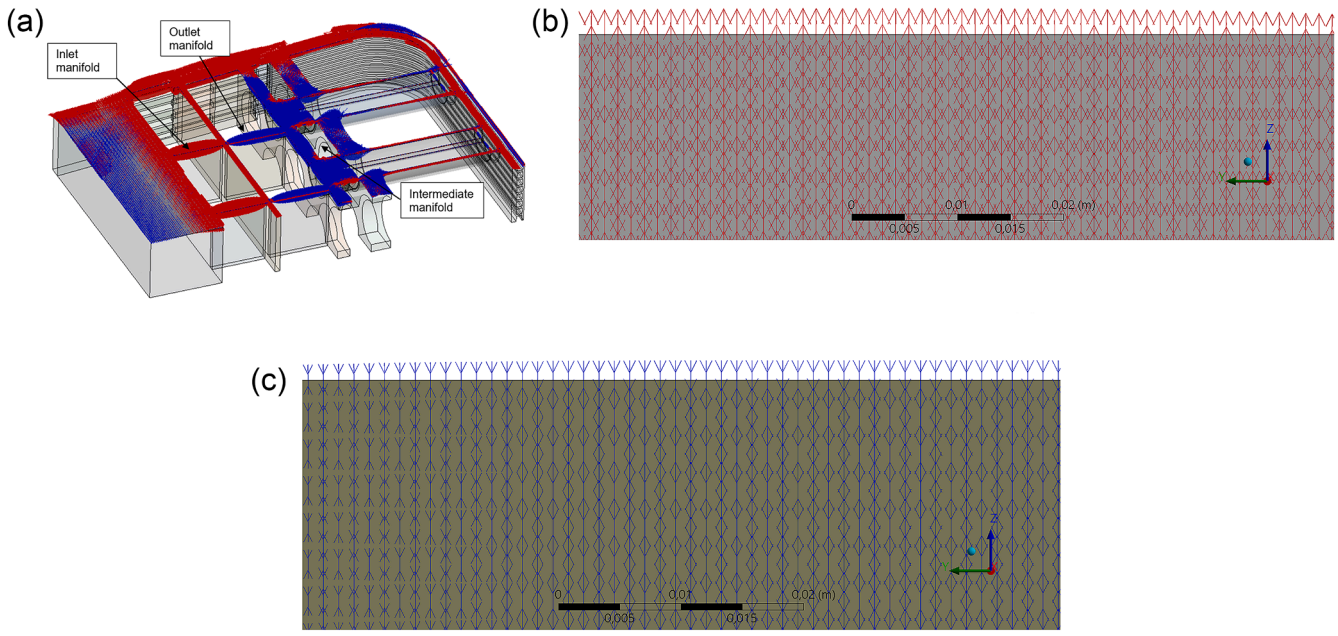

Fig. 20. Vector principal stress (initial design); a) Global view; b) Inlet manifold zoom (traction); c) Outlet manifold zoom (compression).

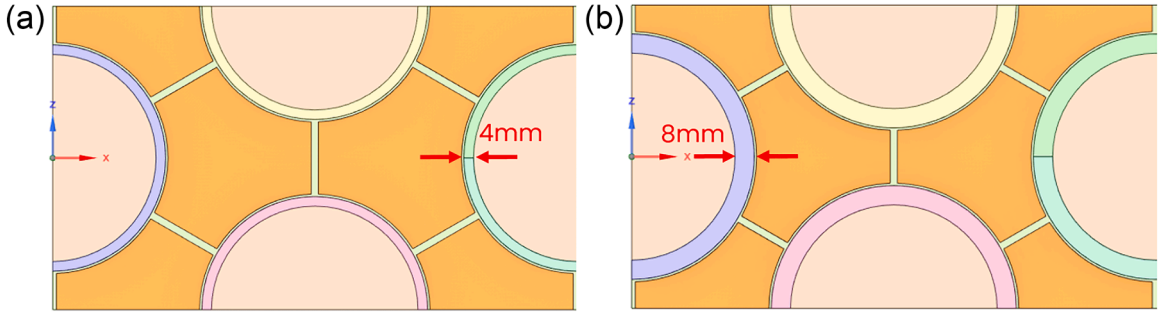

Fig. 21. Cross section on pressure tube and TiBe; a) 4 mm wall thickness; b) 8 mm wall thickness.

Table 9
Thermal analysis results – Pressure tube.

Pressure tube wall thickness (mm)	Minimum temperature (°C)	Maximum temperature (°C)	Temperature difference (°C)	Thermal gradient (°C/mm)
4 (initial design)	478.4	491.6	13.2	3.31
6	479.4	498.5	19.1	3.18
8	480.0	504.4	24.4	3.06

4.3. Pressure tube

The third and last analysed area is the lateral pressure tube. The criterion S_{em} associated with primary and secondary membrane stress is not satisfied for the PT_1 path, as previously described in figures 3 and 4. As for the manifold walls, the objective here is to assess the impact of the pressure tube thickness on primary and secondary stress.

To mitigate the risk of local overheating, the gap specified in Figure 8 (1 mm) is maintained for all designs studied. The design optimisation process consists in increasing the pressure tube thickness by increasing the external diameter (see Fig. 21).

This modification implies a reduction in the volume of neutron multiplier, with possible consequences on the capability of the BB to breed tritium. This will have to be carefully considered and later validated by neutronics calculations.

The results of the thermal analysis are detailed in Table 9. The minimum temperature, which is on the inside of the tube, does not vary with thickness. The maximum temperature increases (external diameter) with thickness, leading to an increase in the temperature difference. However, this slight increase is compensated by the increase in thickness and the thermal gradient remains globally constant. Induced thermal stress is not expected to vary significantly.

The thermomechanical results are shown in Table 10. The thickness of the pressure tube in the initial design is 4 mm. The red colour indicates that the criterion is exceeded.

Table 10
$\overline{P_m + Q_m}$/Sem(T,G) – pressure tube.

Pressure tube wall thickness (mm)	Neutron multiplier volume ratio	$\overline{P_m + Q_m}/S_{em}$
4 (initial design)	1	1.90
6	0.91	1.41
8	0.81	1.12

The results improve as the thickness increases (reduction of the primary contribution in the sum), but the S_{em} criterion is still not achieved. These results can be explained by the fact that the primary membrane stress P_m decreases with increasing thickness, while the secondary membrane stress Q_m remains unchanged (constant thermal gradient as a function of thickness as previously explained). It suggests that a thickness of 10 mm would probably allow the criterion to be satisfied.

On the other hand, a further reduction of the neutron multiplier volume (already reduced by about 20 % for an 8 mm thickness) could become critical for the BB behaviour and the maximum pressure tube temperature could increase to about 510 °C (by extrapolation). In the case that the external diameter cannot be increased, a modification of the internal diameter should be investigated.

It has to be mentioned that for the stress allowable Sem for the damage mode of Immediate Excessive Deformation (IED) with effect of irradiation (SI) is very conservative due to lack of irradiation data. This damage mode shall be reassessed when more irradiation data are available.

5. Conclusions

pppppThermomechanical studies on the initial CD of HCPB BB have highlighted that some RCC-MRx criteria were not satisfied mainly on three areas. These areas are then finely analysed and design improvements are proposed and assessed.

The first area is the SW and the radius fillet that joins it with the FW. The reduction of the flow cross section (reduced from 12×12 mm^2 to 10×10 mm^2), combined with the inward shifting of the FW cooling channels, allows compliance with the S_m criteria, even if the local temperature increases while remaining below the Eurofer temperature limit. However, with regards to the criterion S_{em} associated with membrane stress $\overline{P_m + Q_m}$, the suggested modifications do not enable the admissible value to be achieved, particularly regarding the SW. One further possible solution would be to increase the SW thickness. Another optimisation is the inclusion of a stiffening plate close to the radius fillet, in order to increase the stiffness and reduce the bending stress.

With regards to the second area, the manifold walls, the initial thickness of 10 mm enables the S_m criteria to be satisfied, and this thickness must not be reduced. When the thickness increases, the criterion S_{em} associated with the membrane stress $\overline{P_m + Q_m}$ improves slightly but the result remains unsatisfactory. One possible solution to investigate would be to rearrange the different manifolds in order to achieve a more homogeneous temperature field and a reduction in thermomechanical stresses.

Concerning the third area, the pressure tube, increasing its thickness (by increasing the external diameter) will result in notable improvements. It appears that the S_{em} criterion can be reached with an expected thickness of 10 mm. However, it should be noted that this modification will also reduce the tritium production efficiency (reduction of the volume of the neutron multiplier). Due to lack of irradiation data, the stress allowable S_{em} for the damage mode of Immediate Excessive Deformation (IED) with effect of irradiation (SI) is very conservative.

As presented, some design improvements in terms of mechanical performance are still expected. Further modifications are proposed and will be assessed. Another interesting but very constraining solution that could be efficient would be to further homogenize the temperature field by modifying and improving to the cooling layout (cooling channels, mass flow rate, coolant temperature…,…).

The validation of all criteria presented in this paper is mandatory before proceeding with further study and analysis of others RCC-MRx criteria (such as creep or cyclic loadings). Alternative potential solution to those presented in this paper would be to use an inelastic analysis as suggested in [9] which may help to gain margins. It could be interesting to perform these kind of analysis in the future.

CRediT authorship contribution statement

Brahim Chelihi: Writing – review & editing, Writing – original draft, Software, Resources, Methodology, Investigation, Formal analysis, Data curation, Conceptualization. **Christophe Garnier:** Writing – review & editing, Writing – original draft, Software, Resources, Methodology, Investigation, Formal analysis, Conceptualization. **Julien Aubert:** Writing – review & editing, Validation, Supervision, Project administration, Funding acquisition. **Guangming Zhou:** Writing – review & editing, Project administration.

Declaration of competing interest

The authors declare that they have no known competing financial interests or personal relationships that could have appeared to influence the work reported in this paper.

Acknowledgments

This work has been carried out within the framework of the EUROfusion Consortium, funded by the European Union via the Euratom Research and Training Programme (Grant agreement no 101052200—EUROfusion). Views and opinions expressed are however those of the author(s) only and do not necessarily reflect those of the European Union or the European Commission. Neither the European Union nor the European Commission can be held responsible for them.

Data availability

The authors do not have permission to share data.

References

[1] T. Donné, European research roadmap to the realisation of fusion energy, 2018. ISBN: 9783000611520.
[2] G. Federici, et al., An overview of the EU breeding blanket design strategy as an integral part of the DEMO design effort, Fusion Eng. Des. 141 (2019) 30–42, https://doi.org/10.1016/j.fusengdes.2019.01.141.
[3] F.A. Hernández, P. Arena, L.V. Boccaccini, I. Cristescu, A. Del Nevo, P. Sardain, G. A. Spagnuolo, M. Utili, A. Venturini, G. Zhou, Advancements in designing the DEMO driver blanket system at the EU DEMO pre-conceptual design phase: overview, challenges and opportunities, Nucl. Eng. 4 (3) (2023) 565–601, https://doi.org/10.3390/jne4030037.
[4] G. Zhou, F.A. Hernández, P. Pereslavtsev, B. Kiss, A. Retheesh, L. Maqueda, J. H. Park, The European DEMO helium cooled pebble bed breeding blanket: design status at the conclusion of the pre-concept design phase, Energies 16 (2023) 5377, https://doi.org/10.3390/en16145377.
[5] G. Zhou, et al., Overview of the design activities of the EU DEMO Helium cooled Pebble Bed breeding blanket, in: 15th International Symposium on Fusion Nuclear Technology (ISFNT 2023), Las Palmas de Gran Canaria, Spanien, Sept.2023, pp. 10–15, https://doi.org/10.5445/IR/1000163586.
[6] RCC-MRx édition 2018.
[7] Ansys Workbench 2022 R2.
[8] G. Aiello, J. Aktaa, F. Cismondi, G. Rampal, J.-F. Salavy, F. Tavassoli, Assessment of design limits and criteria requirements for Eurofer structures in TBM components, J. Nucl. Mater. 414 (1) (2011) 53–58, https://doi.org/10.1016/j.jnucmat.2011.05.005. Volume.
[9] A. Retheesh, F.A. Hernández, G. Zhou, Application of inelastic method and its comparison with elastic method for the assessment of In-box LOCA event on EU DEMO HCPB breeding blanket cap region, Appl. Sci. 11 (2021) 9104, https://doi.org/10.3390/app11199104.